Contactless Robotic Micromanipulation in Air Using a Magneto-acoustic System

Omid Youssefi, Student Member, *IEEE*, and Eric Diller, *Member, IEEE*

Abstract— **Precise and dexterous handling of micrometer to millimeter-scale objects are the two crucial and challenging factors for micromanipulation, especially in the fields of biotechnology where delicate microcomponents can be easily damaged by contact during handling. Many complex microrobotic techniques, scaling from fully autonomous to teleoperated, have been developed to address the limitations individually. However, a scalable, reliable, and versatile method which can be applied to a wide range of applications is not present. This work uniquely combines the advantages of magnetic and acoustic micromanipulation methods to achieve three-dimensional, contactless, and semi-autonomous micromanipulation, with potential for full automation, for use in microassembly applications. Solid and liquid materials, with sizes less than 3 mm (down to 300 μm), are handled in a cylindrical workspace of 30 mm in height and 4 mm in diameter using acoustic levitation while an externally applied magnetic field controls the orientation of magnetically active components. A maximum vertical positioning RMSE of 1.5% of parts length was observed. This paper presents the concept, design, characterization, and modeling of the new method, along with a demonstration of a typical assembly process.**

Index Terms—**Micro/Nano Robots, Dexterous Manipulation, Automation at Micro-Nano Scales, Assembly, Telerobotics and Teleoperation.**

I. INTRODUCTION

MICROMANIPULATORS are small-scale systems that aid human operators to perform tasks through guided physical interaction with small objects. Recent studies have allowed for advancement toward achieving necessary levels of accuracy and precision. However, the dexterity of the human hand has been the most challenging aspect for roboticists to achieve. There has been a significant number of studies, such as [1], that focus on approaching this dexterity with automation capability. For applications requiring a high level of dexterity, a skillful human hand with tweezers under the microscope has been shown to be the most effective solution.

However, factors such as the need for highly skilled personnel, high speed, and high precision have posed significant challenges in the field.

For high-precision micromanipulation, microtweezers and microgrippers such as [2] and [3] have been developed which are capable of performing tasks at the cellular level. However, because of direct and concentrated contact [4], high risk of damage is present during grasping, for both elastic and inelastic objects. This damage can be reduced using feedback to adjust the contact forces during gripping but, not eliminated. Also, on the microscale (part sizes below 1 mm), the detection, grasping, and especially releasing are difficult as the viscous and surface contact forces dominate the inertial forces. Thus, releasing microcomponents after grasping is challenging. Studies, such as [5] and [6], have investigated this challenge and developed point-probes to reduce the surface area thereby reducing the grasping adhesion. A closed-loop actuation of the probes is required to perform manipulation tasks, which increase complexity. Also, since the use of onboard power for mobile microrobots at this scale is highly impractical [7], contactless micromanipulation methods have proven effective. Therefore, many contactless micromanipulation methods have been developed that use acoustic waves [8], optical tweezer [9], magnetic actuation [10] and [7], and others that provide application-specific methods with distributed grasping force reducing the contact damage. From these noncontact methods, micromanipulation using magnetics and acoustics have especially gained recent interest due to their precision, versatility, and utility for a wide range of applications. However, high levels of dexterity, as well as precision, have been rarely demonstrated.

Acoustophoretic methods use sound pressure to envelope both liquid and solid particles to compensate for weight which allows for a wide range of possibilities for actuation since the surface contact forces are eliminated as the parts are levitated off the surface. Many studies such as [11] have demonstrated in-air acoustic handling of matter for positioning and orienting of a wide range of objects and droplets for applications ranging from biotechnology to chemistry. Holographic acoustic manipulation of levitated objects [12] also has been reported. However, limitations such as the lack of orientation control over the levitated components and parallel handling of components have limited the adoption of these methods.

Micromanipulation methods that use magnetic actuation such as [13], [14], and [15] have enabled similar and even more advanced capabilities. In these systems, the weight of a magnetic object (e.g., a microgripper) is compensated by the presence of a magnetic gradient field in which, the magnetic
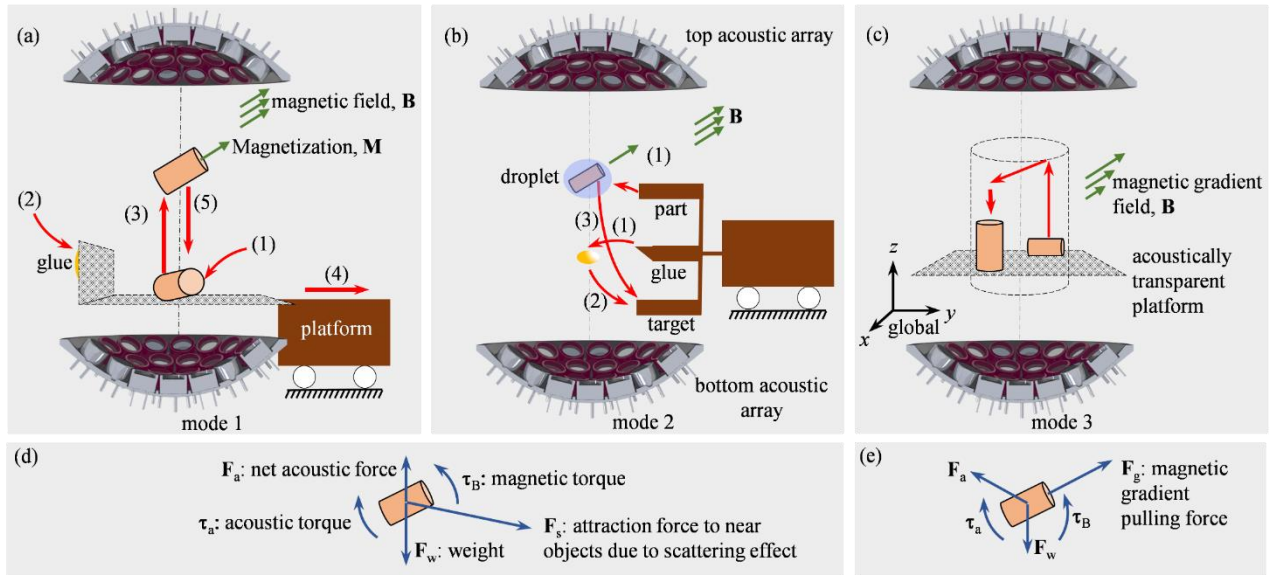
Fig. 1. Conceptual schematic showing the micromanipulation method with different modes of assembly (red arrows indicate movement): (a) mode 1: pick-and-place assembly using a two degree-of-freedom moving platform (*x* and *y* positioning); (b) mode 2: stacked assembly utilizing simultaneous multi-level levitation; (c) mode 3: pick-and-place assembly utilizing magnetic gradient for *x* and *y* positioning (cylindrical workspace); (d) and (e) free-body diagram showing forces and torques applied on the components while being levitated.

objects experience a force in the direction opposite to that of gravity. According to the Earnshaw's theorem, this configuration is inherently unstable. Therefore, these methods must use real-time feedback with advanced controllers to control the position. However, the stability margin is narrow, a high-gradient field is required, and the methods are applicable only to materials that possess a certain degree of magnetic property.

Unlike micromanipulation in liquid, which benefits from damping of undesired movement, and because of high surface forces on the microscale, in-air micromanipulation is difficult, and no versatile method exists for performing micromanipulation tasks on different material types while providing the required capabilities for precision assembly. For the first time, we present a versatile method addressing the most challenging problems for in-air micromanipulation by combining the advantages of magnetic and acoustic fields with a demonstration of robotic microassembly.

II. CONCEPT AND METHOD

In this section, we introduce the concept and the fundamental principle behind the new micromanipulation method for three-dimensional microassembly in the air.

A. Magneto-acoustic Micromanipulation Concept

Micromanipulation is achieved by physical interaction through the application of forces and torques on rigid, flexible, and liquid objects. In this work, a custom-designed acoustic field provides discrete levitation zones where parts can stably levitate mid-air. By adjusting the phase difference between the acoustic emitter elements, these levitation zones move axially in space up or down (vertical positioning). An externally applied magnetic field actuates the magnetically-active components to either self-assemble or to act as a magnetic carrier or backpack to other nonmagnetic components. In a

typical assembly process, parts can be introduced to the system in two main ways: direct placement on an acoustically transparent moving platform (step (1) in Fig. 1(a)); and in-situ delivery using an encapsulating droplet with quick evaporation rate (step (1) in Fig. 1(b)). Parts are then manipulated to desired poses and are placed onto a fixed or a mobile target via attraction force generated by the scattering of the acoustic waves.

This hybrid system is advantageous over either magnetic or acoustic systems alone in that it can manipulate multi-type materials (solid and liquid) both serially and in parallel, use relatively low acoustic and magnetic field amplitudes, and it decouples the position and control actuation for simplifying handling and reducing the complexity of the overall system.

B. Modes of Operation

The assembly can be performed using three modes depending on the specific application needs. Fig. 1 shows the three modes of assembly. In the first mode: (1) part is placed on a moving and an acoustically transparent platform (e.g., fine wire mesh or acoustic cloth); (2) a minute amount of glue is placed on the target zone either using a droplet generator or by direct contact; (3) the part is lifted using acoustic field and oriented using the magnetic field; (4) platform is positioned according to the assembly plan; (5) part is placed onto the target area by platform movement. In this work, this mode is used to perform the microassembly demonstrations. Modes two and three were investigated experimentally and are shown in the supplementary video.

The free-body-diagram is shown in Fig. 1(d) and 1(e) show the dynamics acting on a levitated object. Although the governing equations are introduced in section III, it is critical to first establish the mechanism by which these forces and torques are utilized during assembly. The axial acoustic levitation force balances the weight of the component.

Components within the acoustic field experience different pressure magnitudes across their outer surfaces, and therefore one can determine the net force (F_a) applied to the component by surface integration. This force is in the axial direction for the first two modes and with a radial component in mode 3. Depending on the field distribution, the objects also experience lateral forces. Unlike levitation achieved by magnetic field gradients, this levitation method is stable without feedback and applies to many material states and types.

C. Microassembly Sequence Planning

A sequence of assembly task instructions must be generated a priori for a successful and controllable process. A typical assembly program consists of single-task instructions for the system to execute. For example, a pick-and-place operation can be divided into multiple instructions: (1) move component into the levitation zone via the platform; (2) activate the acoustic transducers to specific amplitude suitable for the component properties; (3) lift the component by adjusting the phase difference; (4) orient the component by applying magnetic torque (if geometry dependent); (5) move platform to target position; and (6) approach the component by moving the platform until the acoustic scattering attraction force results in coalescence between the component and the assembly zone. In order to establish a workflow, part properties must be considered. Fig. 2 shows the individual part parameters that are considered in a typical assembly planning. The shape definition is the input to the system where the final description of the assembled shape is provided. Then, the iterative process of instruction sequencing is implemented to generate the instructions. Then, the assembly program is generated and executed by the system sequentially to form the final product. This workflow generation allows for optimization for increased efficiency of assembly.

III. DESIGN, MODELLING, AND CHARACTERIZATION

In this section, we introduce the design and present the physical modeling followed by system characterization.

A. Acoustic Field Generation

In order to establish a stable configuration of the acoustic waves for levitation, the acoustic element type and location must be carefully selected and designed. One way to achieve this is to use a resonant cavity consisting of a Langevin-style ultrasonic transducer along with a curved reflector such as in [1] and [2]. However, significant effort is required to tune the system to the stringent operating conditions finely. Use of transducer-reflector setup was explored, however; because of unsafe high driving voltage (>100V) and tuning instabilities, this choice was not promising. Another method to achieve levitation is to use a non-resonant single-axis system, such as one suggested in [15]. Unlike the transducer-reflector setup, this system consists of many small ultrasonic transducers. As shown in Fig. 4(a), 37 40-kHz transducers (MSO-P1040H07T) are arranged in a closely-packed fashion onto two opposing spherical domes with an emitting surface radius of 48.8 mm
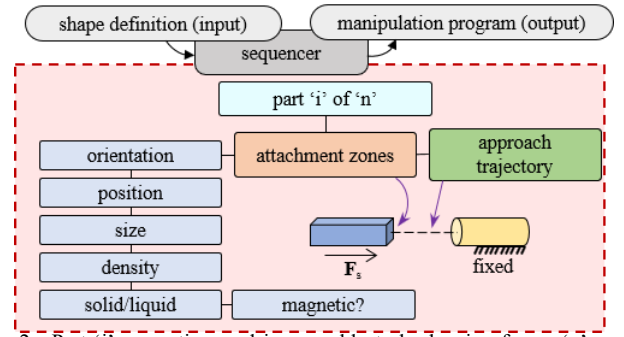

Fig. 2. Part 'i' properties used in assembly task planning for an 'n' part assembly

(the focal length of the array). The two domes are spaced such that the center of curvature of each dome is coincident to achieve equal distances between transducers and the center where the desired levitation zone is located. This configuration simplifies the driving circuitry required since all transducers on either side are driven in parallel with a 40 kHz square wave signal at a low voltage (<30 V_{pp}) by an H-bridge circuit powered by a DC power supply. In this configuration, the sound waves from either side interact and produce a similar pattern to a transducer-reflector design with the advantages of being robust to temperature changes and the ability to change the driving phase resulting in axial (vertical) position control of levitated objects. The transducer displacement amplitude was measured using a laser vibrometer (PSV-500) across 5-12VDC driving voltages, and the acoustic intensity and power were evaluated. The result of this characterization is shown in Fig. 3. The knowledge of the acoustic pressure and velocity field distributions allows one to design and find the locations in space where parts can levitate, and to predict and design payload capacity. According to Gor'kov [16], by knowing the sound pressure, p, and velocity distributions, $\mathbf{v}$, the acoustic potential energy, U, for a small sphere of radius R which is much smaller than the wavelength of sound λ can be calculated by

$$U = 2\pi R^3 \left(\frac{\langle p^2 \rangle}{2\rho_0 c_0^2} - \frac{\rho_0 \langle \mathbf{v} \cdot \mathbf{v} \rangle}{2} \right), \tag{1}$$

where ρ_0 and c_0 are the density of air and the speed of sound in air, respectively (the parameters in angle brackets indicate time-averaged values). After evaluating the acoustic potential
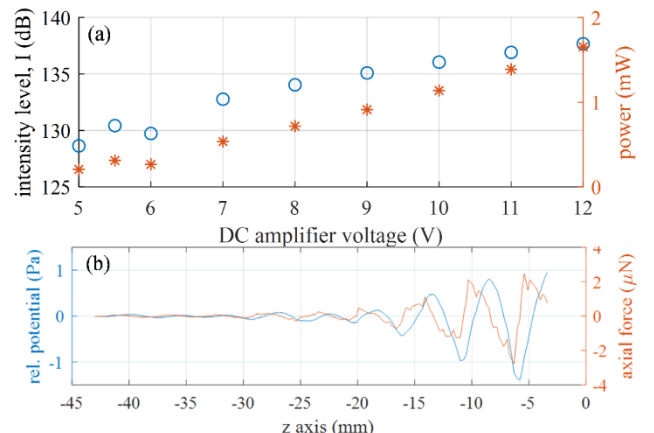

Fig. 3. System characterization results: (a) acoustic intensity level and power of a single 40 kHz transducer and (b) simulated relative acoustic potential and axial levitation force results

distribution within the region of interest, the location of levitation, or the pressure nodes, as well as forces acting on the levitated objects is $F_a = -\nabla U$. The pressure and velocity distribution can be found using analytical models and by simulation. To calculate the distributions analytically, one can assume the closely-packed transducers to resemble a uniform concave emitting surface. With this assumption, the pressure distribution on the central axis of a focusing radiator can be calculated by the real part pressure equation in [17]. To experimentally determine the levitation force, a 2.71 mm Styrofoam sphere was levitated. The driving voltage was reduced to 5.5 V at which, the sphere dropped. A normal surface velocity of about 0.21 m/s was evaluated by interpolation in Fig. 3 and used in simulation to verify the experiment. The pressure and velocity distributions were found using ANSYS harmonic simulation with the Acoustic ACT to verify the simplified model and to predict the levitation forces. The geometry was modeled and a perfectly-matched-layer (PML) boundary condition was applied to the outer surfaces. A speed of sound of 340 m/s and air density of 1.2 kg/cm^3 were applied to the acoustic bodies. The acoustic pressure and velocity distribution were extracted from a cross-sectional surface cutting the design in half and the relative acoustic potential (Eq. (1)/ $2\pi R^3$) was calculated and the surface plot of the result is shown in Fig. 4(a). The regions with the lowest potentials (blue color) are the potential wells that objects will levitate. The analytical and simulated pressure on the central axis are shown in Fig. 3(b). The pressure nodes coincide (zero crossings) indicate the location of the levitation zones. The results from the analytical model and the simulation are well-matched in phase. The amplitudes slightly vary (RMSE = 369 Pa) between the results, which is expected. The analytical model assumes a uniform spherical radiating dome, while in the simulation, the actual geometry of the transducers was modelled with voids in between the transducers resulting in a lower amplitude. To verify the simulation results, a Schlieren image was taken using a custom fabricated setup. The pressure distribution, as viewed from the side, is illustrated in Fig. 4(c) with dark regions being the areas of high acoustic pressure. Using model optimization, a desired distribution pattern can be reliably achieved. When small objects ($R \ll \lambda$) are introduced within the field, the acoustic waves scatter around the object. If larger objects are introduced, the field distribution and magnitude noticeably vary. In addition, two nearby objects within the acoustic field will experience an attraction force due to the unbalanced wave scattering as described in [11]. This is the mechanism by which the parts are assembled (shown in Fig. 2 by F_s).

B. Magnetic Field

As objects scale down, the ability of the acoustic field for providing orientation control diminishes as a result of approaching the wavelength. Moreover, the orientation of symmetrical objects (e.g., a sphere) cannot be controlled by the acoustic field because of balanced torque. Thus, for orientation control, it is required that the object under manipulation possess either a permanent or temporary
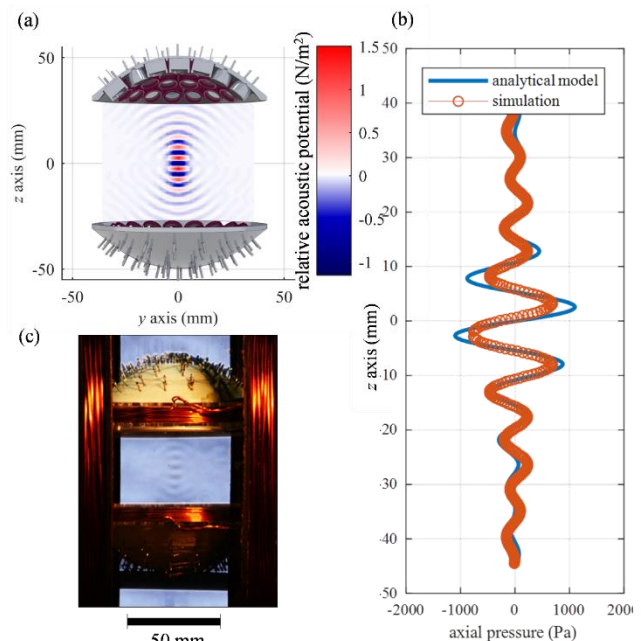

Fig. 4. Determination of acoustic field distribution for levitation zone spacing: (a) plot of relative acoustic potential with superimposed 3D render of transducer arrays on scale: top is a cross-sectional cutout view and bottom is the side view with transducers arranged inside the dome; (b) verification of simulation result with the analytical model, normalized maximum pressure field on central axis (RMSE = 369 Pa); and, (c) optical refractive visualization of density variation using Schlieren imaging.

magnetization (soft magnets). The magnetic torque, $\tau_B = \mathbf{m} \times \mathbf{B}$, where $\mathbf{m}$ is the magnetic moment, and $\mathbf{B}$ is the magnetic flux density, is a two-degree-of-freedom actuation, which allows for orientation control while being levitated and assembled. Since the resistive torques and forces are negligible during levitation, a minute magnetization is sufficient to actuate the components. Automated orientation control is possible and demonstrated under vision feedback. Likewise, a magnetic force $\mathbf{F}_g = (\mathbf{m} \cdot \nabla)\mathbf{B}$ can be applied which enables the gradient pulling of magnetically-active components either to apply force required for assembly or to position in xy within the cylindrical workspace as shown in Fig. 1(c). This functionality has been demonstrated in the supplementary video. It is also possible to perform assisted levitation for denser magnetic objects by providing a magnetic force directed toward $+z$ to augment the acoustic radiation force. Unlike levitation achieved by the magnetic field alone, which requires real-time feedback [15] and cumbersome calibration, the acoustic well provides a cushion for disturbances which enables open-loop levitation. For the first time, a spherical neodymium N50 magnet with a diameter of up to 3 mm was stably levitated open-loop with low field magnitudes.

IV. RESULTS AND DISCUSSION

A. Experiment Setup – Required Modules

The system is comprised of actuation, detection, positioning, and user control interface modules. Fig. 5 shows a side view of the system in detail. The actuation module consists of 4 pairs of orthogonally nested rectangular coils with three pairs providing a uniform magnetic field of 3 mT
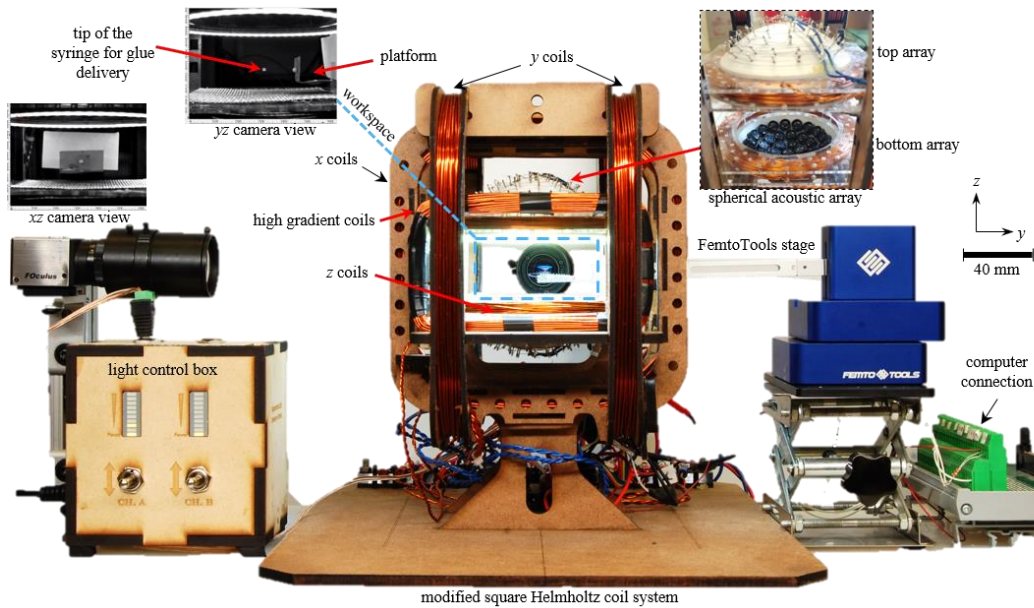
Fig. 5. Experiment setup: the workspace is within the modified Helmholtz coil system. There are 4 pairs of orthogonally nested rectangular coils generating the uniform magnetic field. Cameras look directly on *xz* and *yz* planes.

across a workspace with dimensions of 30 × 40 × 40 mm. The fourth pair (the high gradient coils in Fig. 5) provide a magnetic gradient with a maximum magnitude of about 0.4 T/m necessary for radial positioning. The magnitude of the field is proportional to the driving current which is controlled by eight amplifiers (Advanced Motion Controls, 30A8) with commands sent by a Linux operation system through a PCIe I/O board (Sensoray, Model s826). The detection module is comprised of two cameras (FOculus, FO123TB) aligned perpendicular to *xz* and *yz* planes and the images are analyzed using vision algorithms for detection of the pose of the levitated objects. The acoustically transparent platform (0.2 mm pitch Aluminum wire mesh grid), which is mobile, is mounted on a positioning module (FemtoTools precision *xyz* stage). The user provides inputs through a custom-designed graphical user interface to the system teleoperating some tasks. In this work, the orientation and radial and axial positions are automated.

B. Manipulation Characterization – Position and Force

A microsphere with a diameter of 920 μm (Cospheric BKPMS-1.2) was levitated, and three stepwise *z* positions were selected to characterize *z* position precision and stability. Fig. 6(a) shows the *z* position control outputs with RMSE of 0, 0.018, and 0.014 mm for the three respective step inputs. The vertical traversal speed was limited to about 3.5 mm/s by controlling the rate of change of the acoustic phase difference between the top and the bottom arrays. This result shows about 1.5% of parts length maximum in-situ disturbance mean error, which is negligible. Fig. 6(b) shows the result of orientation control of an assembled magnetic beam onto a post with uncured glue. The measured and commanded angles follow closely since the magnetic field can be adjusted with high precision by the electromagnetic coil system. All measurements were taken using vision analysis. In order to determine the payload capacity, the axial (*z*-direction) and

radial (*x* or *y*) forces on a levitated 2.7 mm Styrofoam sphere were measured using FemtoTools stationary force probes (FT-S1000 and FT-G102 for radial and axial measurements, respectively). In this configuration, the axial and radial forces both increased linearly with the driving voltage with the axial force being about two times stronger ash shown in Fig. 6(c). Given a fixed geometry, one can use this method to determine the density of levitated objects by comparing the drop voltage with the calibrated force curve. Assuming a density of 300 kg/m^3, a theoretical mass of 31 μg of the levitated sphere from the drop experiment in section III is evaluated. The weight of about 34 μN is interpolated from Fig. 6(c) which matched closely with that of the prediction verifying the force measurement accuracy.

C. Demonstration of Microassembly

Using the first mode of assembly, two assembly programs for generating shapes of an Inuksuk (a traditional figure made of piled stone) and the letters UT were followed to fabricate the shapes with automated orientation control. The parts,
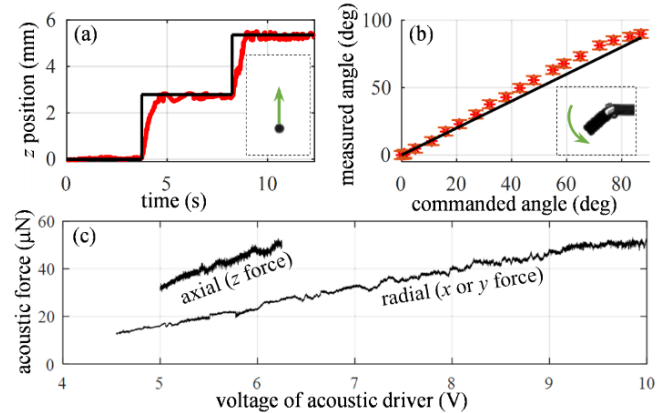

Fig. 6. Micromanipulation characterization results: (a) acoustically actuated step *z* position input with measured position (green arrow points toward +*z*); (b) orientation response with magnetic actuation; and (c) radial and axial (*y* and *z*, respectively) forces on a 2.7 mm Styrofoam sphere.
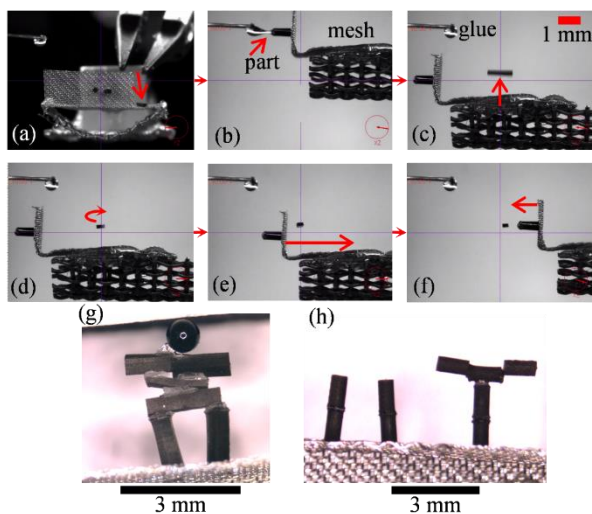
Fig. 7. Microassembly demonstration (arrows indicate movement direction): (a) part placement using tweezer; (b) glue pick up from a 30-gauge dispensing needle; (c) part lift-off via activation of acoustic field; (d) part orientation control using magnetic field; (e) positioning of platform; (f) approach trajectory; (g) seven-component assembly of an Inuksuk figure; and (h) nine-component assembly of UT shape.

which are magnetic composite materials, contain ultra-fine magnetic powder (MQFP) and polyurethane 1:31 ratio vol./vol. and a density of 1.35 g/cm^3. Parts for UT shape are all cylinders of diameter 0.5 mm and length of 1 mm and for Inuksuk, 1 mm sphere and rectangular beams of arbitrary sizes. These components were magnetized by exposure to 1.1 T of magnetic flux density. These components were assembled using the steps shown in Fig. 2 with the application of superglue. Fig. 7 shows the sequence of the assembly process along with the final assembled shapes. The orientation, as well as the attachment zones, were determined by both the shape definition and the magnetization direction of the parts. Smaller-sized objects were also manipulated using the same system with sizes down to 300μm. A comparative experimental measurement of acoustic pressure was performed to assess the reduction or scattering of waves caused by the acoustically transparent platform (ATP). Results show that there can be a maximum of 2% in reduction of the acoustic pressure amplitude through the ATP. Since the openings on the ATP are uniform, according to Huygens principle, the overall field distribution would be equivalent to the case where ATP is not present.

V. Conclusion

In this paper, a new class of micromanipulation for magneto-acoustic robotic assembly is presented for the first time. Assembly subtask planning, along with the design and characterization of acoustic and magnetic fields, were investigated and the simulated results were confirmed with the analytical models and the experiments. The versatility of this method to effectively manipulate multiple material types and geometries along with automation potential throughout the process is promising for use in applications such as optical catheters production and cell or organism manipulation in biotechnology applications. Orientation control of nonmagnetic objects is not possible with this method,

however; the addition of a magnetic backpack or coating is of interest for future work. Due to the small field magnitudes, there was no observable interference between the magnetic and acoustic systems concerning the field distribution or a significant change in the field magnitude. Unlike previous magnetic or acoustic micromanipulation methods, which use high-intensity fields, this work uses low magnitudes which is advantageous in design and usage. Since all the applied forces scale proportionally with the object size, this method proves to be highly practical for micromanipulation as objects do not experience the high surface adhesion forces. Microassembly in microgravity environments and of sub-millimeter medical devices in biomedical and chemical fields are the most notable areas of interest. Future work will include assembly speed and failure rate characterization.

References

[1] R. L. A. Shauri, N. M. Salleh, and A. K. A. Hadi, "PID position control of 7-DOF three-fingered robotic hand for grasping task," in *Proceedings - 4th IEEE International Conference on Control System, Computing and Engineering*, 2014, pp. 70–74.

[2] A. F. Alogla, F. Amalou, C. Balmer, P. Scanlan, W. Shu, and R. L. Reuben, "Corrigendum to 'Micro-tweezers: Design, fabrication, simulation and testing of a pneumatically actuated micro-gripper for micromanipulation and microtactile sensing,'" *Sensors and Actuators, A: Physical*. pp. 394–404, 2018.

[3] K. Kim, X. Liu, Y. Zhang, and Y. Sun, "Micronewton force-controlled manipulation of biomaterials using a monolithic MEMS microgripper with two-axis force feedback," in *IEEE International Conference on Robotics and Automation*, 2008, pp. 3100–3105.

[4] J. a. Thompson and R. S. Fearing, "Automating microassembly with ortho-tweezers and force sensing," *Proc. 2001 IEEE/RSJ Int. Conf. Intell. Robot. Syst. Expand. Soc. Role Robot. Next Millenn. (Cat. No.01CH37180)*, 2001.

[5] J. D. Wason, J. T. Wen, J. J. Gorman, and N. G. Dagalakis, "Automated multiprobe microassembly using vision feedback," *IEEE Trans. Robot.*, 2012.

[6] D. J. Cappelleri, P. Cheng, J. Fink, B. Gavrea, and V. Kumar, "Automated assembly for mesoscale parts," *IEEE Trans. Autom. Sci. Eng.*, 2011.

[7] E. Diller, J. Giltinan, G. Z. Lum, Z. Ye, and M. Sitti, "Six-degree-of-freedom magnetic actuation for wireless microrobotics," *Int. J. Rob. Res.*, 2016.

[8] F. Guo *et al.*, "Three-dimensional manipulation of single cells using surface acoustic waves," *Proc. Natl. Acad. Sci.*, 2016.

[9] M. C. Williams, "Optical Tweezers : Measuring Piconewton Forces," *Physics (College. Park. Md).*, 2002.

[10] M. P. Kummer, J. J. Abbott, B. E. Kratochvil, R. Borer, A. Sengul, and B. J. Nelson, "Octomag: An electromagnetic system for 5-DOF wireless micromanipulation," *IEEE Trans. Robot.*, vol. 26, no. 6, pp. 1006–1017, Dec. 2010.

[11] D. Foresti, M. Nabavi, M. Klingauf, A. Ferrari, and D. Poulikakos, "Acoustophoretic contactless transport and handling of matter in air.," *Proc. Natl. Acad. Sci. U. S. A.*, vol. 110, no. 31, pp. 12549–54, Jul. 2013.

[12] A. Marzo, S. A. Seah, B. W. Drinkwater, D. R. Sahoo, B. Long, and S. Subramanian, "Holographic acoustic elements for manipulation of levitated objects," *Nat. Commun.*, 2015.

[13] A. Hsu *et al.*, "Diamagnetically levitated Milli-robots for heterogeneous 3D assembly," *J. Micro-Bio Robot.*, 2018.

[14] E. Shameli, M. B. Khamesee, and J. P. Huissoon, "Nonlinear controller design for a magnetic levitation device," in *Microsystem Technologies*, 2007, vol. 13, no. 8–10, pp. 831–835.

[15] C. Elbuken, M. B. Khamesee, and M. Yavuz, "Design and implementation of a micromanipulation system using a magnetically levitated MEMS robot," *IEEE/ASME Trans. Mechatronics*, vol. 14, no. 4, pp. 434–445, Aug. 2009.

[16] W. J. Xie, C. D. Cao, Y. J. Lü, Z. Y. Hong, and B. Wei, "Acoustic method for levitation of small living animals," *Appl. Phys. Lett.*, vol. 89, no. 21, p. 214102, Nov. 2006.

[17] M. A. B. Andrade, A. L. Bernassau, and J. C. Adamowski, "Acoustic levitation of a large solid sphere," *Appl. Phys. Lett.*, vol. 109, no. 4, p. 044101, Jul. 2016.

[18] A. Marzo, A. Barnes, and B. W. Drinkwater, "TinyLev: A multi-emitter single-axis acoustic levitator," *Rev. Sci. Instrum.*, vol. 88, no. 8, p. 085105, Aug. 2017.

[19] L. P. Gor'kov, "On the Forces Acting on a Small Particle in an Acoustical Field in an Ideal Fluid," *Solviet Phys. Dokl.*, vol. 6, no. 1, p. 773, 1962.

[20] H. T. O'Neil, "Theory of Focusing Radiators," *J. Acoust. Soc. Am.*, 1949.